SCIENTIFIC REPORTS

OPEN

SUBJECT AREAS:
SOLAR CELLS
SOLAR ENERGY AND PHOTOVOLTAIC TECHNOLOGY
RENEWABLE ENERGY

Received
10 July 2014

Accepted
12 January 2015

Published
11 February 2015

Correspondence and requests for materials should be addressed to K.K. (kimkk@ewha.ac.kr)

Efficient Organic Photovoltaics Utilizing Nanoscale Heterojunctions in Sequentially Deposited Polymer/fullerene Bilayer

Jeesoo Seok[1], Tae Joo Shin[2], Sungmin Park[3], Changsoon Cho[4], Jung-Yong Lee[4], Du Yeol Ryu[3], Myung Hwa Kim[1] & Kyungkon Kim[1]

[1]Department of Chemistry and Nano Science, Global Top 5 Research Program, Ewha Womans University, Seoul 120-750, Republic of Korea, [2]Pohang Accelerator Laboratory, Pohang, Kyungbuk 790-784, Republic of Korea, [3]Department of Chemical and Biomolecular Engineering, Yonsei University, Seoul 120-749, Republic of Korea, [4]Graduate School of Energy, Environment, Water, and Sustainability (EEWS), Graphene Research Center, KAIST, Daejeon 305-701, Republic of Korea.

A highly efficient sequentially deposited bilayer (SD-bilayer) of polymer/fullerene organic photovoltaic (OPV) device is developed via the solution process. Herein, we resolve two essential problems regarding the construction of an efficient SD-bilayer OPV. First, the solution process fabrication of the SD-bilayer is resolved by incorporating an ordering agent (OA) to the polymer solution, which improves the ordering of the polymer chain and prevents the bottom-layer from dissolving into the top-layer solution. Second, a non-planar heterojunction with a large surface area is formed by the incorporation of a heterojunction agent (HA) to the top-layer solution. Poly[[9-(1-octylnonyl)-9H-carbazole-2,7-diyl]-2,5-thiophenediyl-2,1,3-benzothiadiazole-4,7-diyl-2,5-thiophenediyl] (PCDTBT) is used for the bottom-layer and phenyl-C71-butyric-acid-methyl ester (PC70BM) is used for the top-layer. The SD-bilayer OPV produced utilizing both an OA and HA exhibits a power conversion efficiency (PCE) of 7.12% with a high internal quantum efficiency (IQE). We believe our bilayer system affords a new way of forming OPVs distinct from bulk heterojunction (BHJ) systems and offers a chance to reconsider the polymers that have thus far shown unsatisfactory performance in BHJ systems.

Organic photovoltaic (OPV) devices have received intense attention due to their low-cost manufacturing[1], ease of processing[2] and mechanical flexibility[3]. These OPVs utilize a bulk heterojunction (BHJ) type photoactive layer where the electron donating polymer and electron accepting fullerene are blended into one layer to form a heterojunction in the bulk film. In order to achieve a large heterojunction area for efficient exciton dissociation, nanoscale phase separation between the polymer and fullerene is desired. Therefore, the BHJ system requires a delicate control of the processing conditions including the blending ratio between the polymer and fullerene, the amount of processing additives, the kinds of solvents used and the thermal annealing temperature.

Analogous to its use in inorganic solar cells, the bilayer structure of a p-type polymer and an n-type fullerene can be utilized for OPVs. A bilayer structure can be prepared by the sequential deposition of polymer and fullerene solutions. Usually, there is interdifussion of polymer and fullerene at the polymer/fullerene interface in the sequentially deposited bilayer (SD-bilayer) of polymer/fullerene. Nevertheless, compared to the blending system, finding the optimum conditions for a SD-bilayer is more straightforward. However, two major requirements first need to be addressed for the satisfactory application of the SD-bilayer to OPVs. First, the top-layer solvent should not destroy the bottom-layer. Since considering the thickness of active layer in OPV devices is usually less than 100 nm, the material in the bottom-layer should have little solubility in the top-layer solvent. Second, the interfacial area at the top-layer/bottom-layer heterojunction should be large enough for efficient exciton dissociation.

Recently, several interesting results regarding a poly(3-hexylthiophene) (P3HT)/phenyl-C_{61}-butyric acid methyl ester ($PC_{60}BM$) SD-bilayer OPV have been reported[4–9]. Dichloromethane (DCM) was used as the solvent for the $PC_{60}BM$ top-layer because DCM does not destroy the P3HT bottom-layer. It was found that partial

penetration of the $PC_{60}BM$ top-layer into the P3HT bottom-layer occurred after thermal annealing at above the glass transition temperature of P3HT. The penetration increases heterojunction area by forming a non-planar heterojunction, which results in an enhancement of the SD-bilayer OPV efficiency. The efficiency of the thermally annealed P3HT/$PC_{60}BM$ SD-bilayer OPV showed comparable efficiency to that of a BHJ OPV device. Recently, an organic solar cell based on a PTB7/$PC_{70}BM$ SD-bilayer was reported[10]. However, the power conversion efficiency (PCE) of the solar cell was found to be around 3%, which is significantly lower than the PCE of a solar cell utilizing a PTB7 : $PC_{70}BM$ BHJ.

The proper solvent for SD-bilayer OPV fabrication must be considered as DCM is not always appropriate to use in every SD-bilayer device of polymer/fullerene due to the various solubilities of different polymers in DCM. For example, PCDTBT is known to exhibit high solar cell efficienc[11] and stability[12,13] when it forms a BHJ with $PC_{70}BM$. However, even though the solubility of PCDTBT in DCM is low (0.54 mg/mL), the solvent almost completely removes the thin PCDTBT film (50 nm), and consequently, constructing a SD-bilayer of PCDTBT/$PC_{70}BM$ is impossible when using a DCM solution.

In this work, we report an efficient SD-bilayer solar cell based on a PCDTBT/$PC_{70}BM$. We have resolved two essential problems: the construction of the SD-bilayer by a solution process and the formation of a heterojunction with a large surface area by introducing an ordering agent (**OA**) and a heterojunction agent (**HA**) to the bottom- and top-layer solutions, respectively. The SD-bilayer OPV utilizing both an **OA** and a **HA** shows PCE of 7.12% with the internal quantum efficiency (IQE) over 90%.

Results and discussions

We investigated whether DCM, the solvent for the $PC_{70}BM$ top-layer, dissolves the PCDTBT bottom-layer by spin-coating DCM onto the PCDTBT layer. The PCDTBT layer was nearly completely removed after spin-coating with DCM. This is ascribed to the amorphous (or less ordered) feature of the PCDTBT chains. In the P3HT/$PC_{60}BM$ SD-bilayer OPV, domains of highly ordered P3HT chains prevent the dissolution of P3HT by blocking DCM penetration. This implies that polymer chains should form ordered domains to successfully construct a polymer/$PC_{60}BM$ SD-bilayer using the sequential solution process. Unfortunately, many of the recently developed low band gap polymers, including PCDTBT, are amorphous due to the bulky alkyl side chains required for the solubility enhancement of the polymers[14–16].

In this respect, two approaches for enhancing the ordering of the polymer chains were executed. First, thermal annealing of the polymer at a proper temperature[17,18] can enhance ordering. Recently, X. Lu *et al.*[19] reported that ordered PCDTBT domains were created after thermal annealing at 200°C. Second, utilizing an **OA** assists in the formation of ordered polymer domains. Proper **OA** selection depends upon the **OA** having a lower vapor pressure and little solubility for the polymer when compared with the host solvent. These properties allow the **OA**, when added to the host solvent, to give the polymer chains more time to achieve an ordered state by reducing the evaporation rate of the host solvent. In addition, when the host solvent has evaporated, the remaining **OA** (poor solvent for polymer) aids in the precipitation of the polymer leading to the formation of ordered polymer domains. We have found several suitable **OA**s for PCDTBT. 1,8-Diiodooctane (**DIO**) was chosen as one **OA** for PCDTBT due to its negligible vapor pressure and the fact that PCDTBT is insoluble. The PCDTBT was dissolved in 99 vol% of chlorobenzene (**CB**) and 1 vol% of **DIO**. For clarity, the PCDTBT layers prepared with this solvent system (1 vol% of **DIO**) and those prepared without **DIO** will be denoted as **PCDTBT(OA)** and **PCDTBT(N)**, respectively, and the thermally annealed PCDTBT will be denoted as **PCDTBT(N–T)**.

Figure 1 shows the absorption intensity change for the PCDTBT films with different preparation methods (Film 1 of Figure 1a). The black lines in Figure 1 b, c and d are absorption spectra of as-prepared **PCDTBT(N)**, **PCDTBT(OA)** and **PCDTBT(N–T)** films, respectively. All the films show similar absorption intensity regardless of the preparation method. This absorption intensity shows that the thicknesses of the PCDTBT films were not affected by the addition of an **OA** or by thermal annealing. Subsequently, the $PC_{70}BM$ DCM

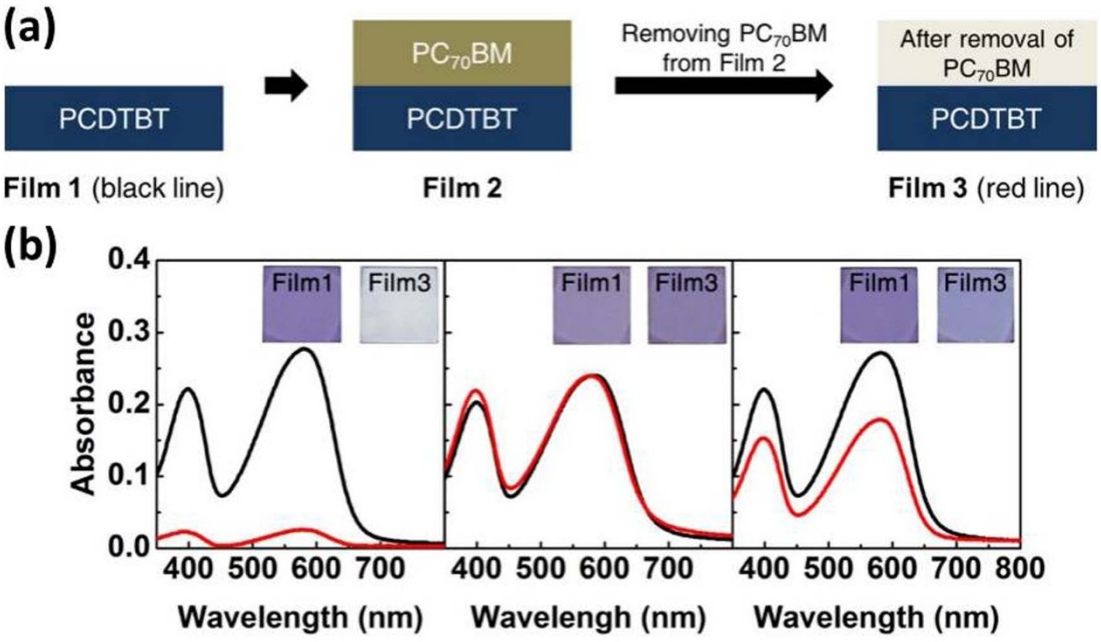

Figure 1 | Preparation procedure of films and the UV-visible absorption spectra of PCDTBT films. (a) Graphical representation of the as-prepared PCDTBT bottom-layer (Film 1), SD-bilayer of PCDTBT/$PC_{70}BM$ (Film 2) and PCDTBT bottom-layer after removing the $PC_{70}BM$ top-layer from the SD-bilayer (Film 3). (b) UV-visible absorption spectra of PCDTBT(N), (c) UV-visible absorption spectra of PCDTBT(N–T), and (d) UV-visible absorption spectra of PCDTBT(OA). Black lines represent the absorption of Film 1. Red lines represent the absorption of Film 3.

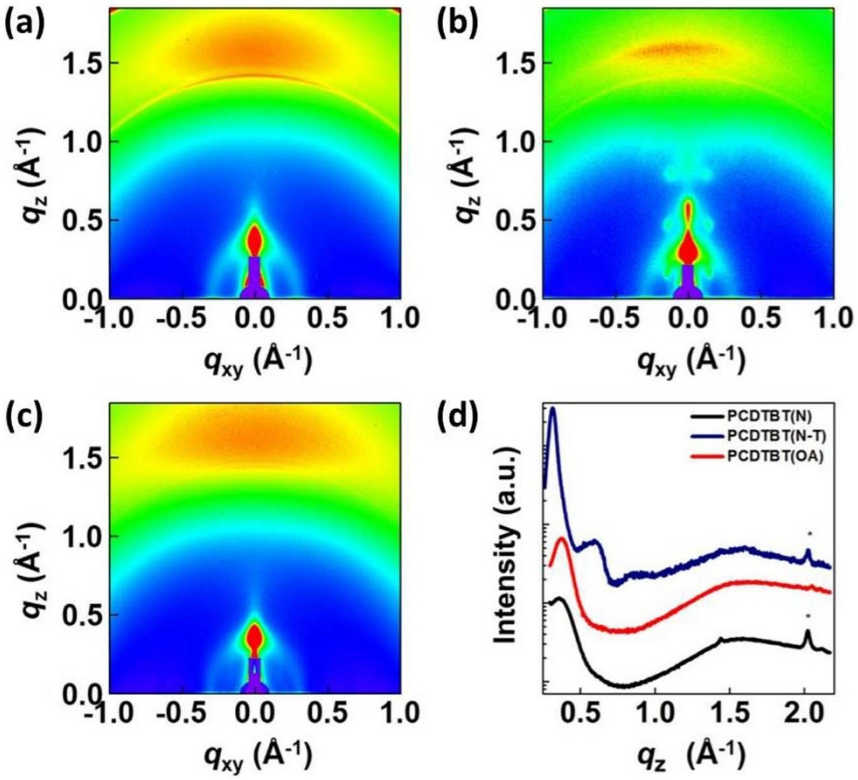

Figure 2 | 2D GIXD images of the PCDTBT films (a–c) and their out-of-plane (q_z) scattering profiles (d). (a) PCDTBT(N), (b) PCDTBT(N–T), and (c) PCDTBT(OA), (d) out-of-plane (q_z) scattering profiles extracted from 2D GIXD patterns of (a–c).

solution was spin-coated on the PCDTBT bottom-layer to form the $PC_{70}BM$ top-layer (Film 2 of the Figure 1a). To verify the thickness of the PCDTBT bottom-layer after spin-coating with $PC_{70}BM$ solution, the $PC_{70}BM$ top-layer was selectively removed using diiodomethane (**DIM**) which is a good solvent for $PC_{70}BM$ and a non-solvent for PCDTBT (Film 3 of the Figure 1a). Red lines in Figure 1 show the absorption spectrum of the corresponding PCDTBT bottom-layer after removing the $PC_{70}BM$ top-layer. The absorption spectra and the photographs in Figure 1b indicate that the **PCDTBT(N)** was almost completely removed by the $PC_{70}BM$ top-layer solution. This is in contrast to the **PCDTBT(N–T)**, which was insoluble in the $PC_{70}BM$ solution (Figure 1c). Figure 1d indicates that a considerable amount (65.8%) of the **PCDTBT(OA)** bottom-layer remained even after spin-coating with the $PC_{70}BM$ solution.

To investigate the ordering and orientation of the polymer chains in the PCDTBT layer, grazing incidence X-ray diffraction (GIXD) experiments were performed. Figure 2a–c shows 2D GIXD images of the PCDTBT layers prepared from the different processing conditions. Two broad peaks were observed for the **PCDTBT(N)** and **PCDTBT(OA)**. According to X. Lu *et al.*[4], the peak at around 1.5 Å^{-1} (4.2 Å) corresponds to the $\pi - \pi$ stacking distance and the peak in the range of 0.355–0.406 Å^{-1} (17.7–15.5 Å) corresponds to the spacing between the polymer chains. Additional peaks between 0.5 Å^{-1} and 1.0 Å^{-1} along the q_z direction were observed from **PCDTBT(N–T)**. These peaks are related to the second- and third-order reflections showing long range ordered structures parallel to the substrate[18]. Figure 2d compares out-of-plane scattering profiles extracted from the 2D GIXD patterns of corresponding films. The peaks marked with an asterisk are caused by indium tin oxide (ITO) diffuse scattering. Their crystallographic information is summarized in Table 1. The calculated coherence length along the q_z axis (surface normal) increased in the order of **PCDTBT(N)** < **PCDTBT(OA)** < **PCDTBT(N–T)**. The coherence lengths of PCDTBT in **PCDTBT(N–T)** and **PCDTBT(OA)** are 380% and 48.3% larger than that of PCDTBT in **PCDTBT(N)**, respectively. The out-of-plane scattering analysis of the PCDTBT layers revealed that the **PCDTBT(N)** did not show significant PCDTBT chain ordering and the **PCDTBT(OA)** showed enhanced chain ordering along the q_z direction. Additionally, the **PCDTBT(N–T)** showed significant enhancement in the PCDTBT chain ordering along the q_z direction. These results suggest that including the **OA** in the PCDTBT solution enhances the chain ordering of PCDTBT implying that **DIO** plays a vital role in the chain ordering of PCDTBT. Consequently, the ordered PCDTBT domains established by the **OA** will be less soluble in the $PC_{70}BM$ solvent, which corresponds well with the UV-visible absorption results in Figure 1. This clearly shows that the incorporation of an **OA** to the PCDTBT solution or the thermal annealing of the PCDTBT film enables the SD-bilayer of PCDTBT/$PC_{70}BM$ to be fabricated by the solution process.

Table 1 | Crystallographic information obtained from the scattering profile of PCDTBT films along the q_z axis

	PCDTBT(N)	PCDTBT(N–T)	PCDTBT(OA)
q (Å^{-1})	0.355	0.314	0.372
d-spacing (Å)	17.7	20.0	16.9
FWHM (Å^{-1})	0.175	0.046	0.118
Coherence length (Å)	32.3	123.0	47.9

The SD-bilayer of PCDTBT/$PC_{70}BM$ was successfully prepared by sequential spin-coating with PCDTBT and the $PC_{70}BM$ solution. The constructed SD-bilayer films were utilized as the active layer in a OPV with the device structure ITO/PEDOT : PSS/PCDTBT/$PC_{70}BM$/TiO_2/Al. Table 2 compares the performance of the SD-bilayer OPV. For clarity, $PC_{70}BM$ layers prepared with DCM will be denoted as **$PC_{70}BM$(N)**. Three different SD-bilayers of **PCDTBT(N)/$PC_{70}BM$(N)**, **PCDTBT(N–T)/$PC_{70}BM$(N)** and **PCDTBT(OA)/$PC_{70}BM$(N)** were used as the active layer of a SD-bilayer OPV, and the solar cell utilizing **PCDTBT(OA)/$PC_{70}BM$(N)**

Table 2 | Solar cell parameters of PCDTBT/$PC_{70}BM$ SD-bilayer OPVs

Bottom-layer (Donor layer)	Top-layer (Acceptor layer)	V_{OC} (V)	J_{SC} (mA/cm^2)	FF	PCE (%)
PCDTBT(N)	**$PC_{70}BM$(N)**	0.84	2.68	0.48	1.09
PCDTBT(N–T)	**$PC_{70}BM$(N)**	0.87	3.02	0.42	1.10
PCDTBT(OA)	**$PC_{70}BM$(N)**	0.94	4.27	0.45	1.82
PCDTBT(N)	**$PC_{70}BM$(HA)**	0.88	5.18	0.63	2.88
PCDTBT(N–T)	**$PC_{70}BM$(HA)**	0.91	7.99	0.51	3.70
PCDTBT(OA)	**$PC_{70}BM$(HA)**	0.90	12.02	0.66	7.12

showed the highest PCE (1.82%) among the three types of devices. The PCE difference was mainly ascribed to the short circuit current density (J_{SC}). However, all SD-bilayer solar cells exhibited similar PCEs, and the values are significantly lower than that of BHJ solar cells, which range from 6.4 to 7.1%[20–22].

There are two possible reasons for these results. First, the low PCEs could be ascribed to the low solubility (4.47 mg/mL) measured for $PC_{70}BM$ in DCM. The solubility is too low for the conformal formation of the $PC_{70}BM$ top-layer on the PCDTBT bottom-layer with a proper thickness. The second reason could be due to the volatility of DCM. The highly volatile DCM will evaporate quickly leaving large domains of $PC_{70}BM$ on the PCDTBT bottom-layer. To investigate this hypothesis, the surface of SD-bilayer of PCDTBT/$PC_{70}BM$ was scanned using atomic force microscopy (AFM). The scanning electron microscopy (SEM) image of the SD-bilayer surface clearly showed large aggregations of $PC_{70}BM$ on the PCDTBT bottom layer with various diameters (Figure 3a). The features of $PC_{70}BM$ domains are exactly matched with the surface morphologies of the PCDTBT bottom-layer after removal of the $PC_{70}BM$ top-layer from the SD-bilayer films of PCDTBT/$PC_{70}BM$ (Figure 3b–d). The large holes with a diameter of around 200–800 nm were observed in all three SD-bilayer films, suggesting that the large domains of $PC_{70}BM$ were formed on the PCDTBT bottom-layer during coating with the $PC_{70}BM$ top-layer and left indentations when the $PC_{70}BM$ domains were removed with **DIM**. The domain size was significantly larger than the exciton diffusion length, which would reduce the exciton dissociation efficiency. This could be a major reason for the poor performance of the PCDTBT/$PC_{70}BM$ SD-bilayer OPVs without concerning the various PCDTBT bottom-layers. In addition, the low fill factor (FF) of the solar cell reflects a significant charge recombination due to an imbalance between electrons and hole transport.

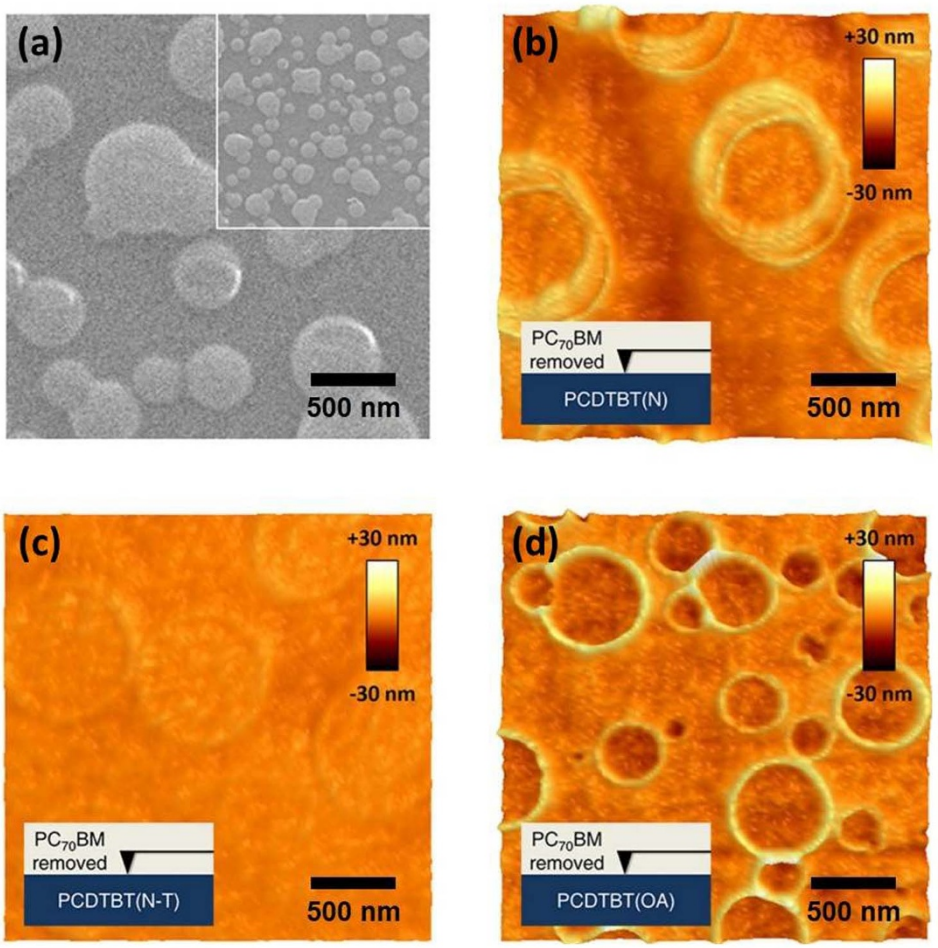

Figure 3 | Surface morphologies of the SD-bilayer of PCDTBT(OA)/$PC_{70}BM$ obtained by SEM (a) and PCDTBT bottom-layers (b–d) obtained by AFM. (a) PCDTBT(OA)/$PC_{70}BM$ SD-bilayer, (b) PCDTBT(N) bottom-layer after removal of the $PC_{70}BM$ top-layer from the PCDTBT(N)/$PC_{70}BM$ film, (c) PCDTBT(N–T) bottom-layer after removal of the $PC_{70}BM$ top-layer from the PCDTBT(N–T)/$PC_{70}BM$ and (d) PCDTBT(OA) bottom-layer after removal of the $PC_{70}BM$ top-layer from the PCDTBT(OA)/$PC_{70}BM$. All the images were obtained by AFM in tapping mode (2.5 μm × 2.5 μm).

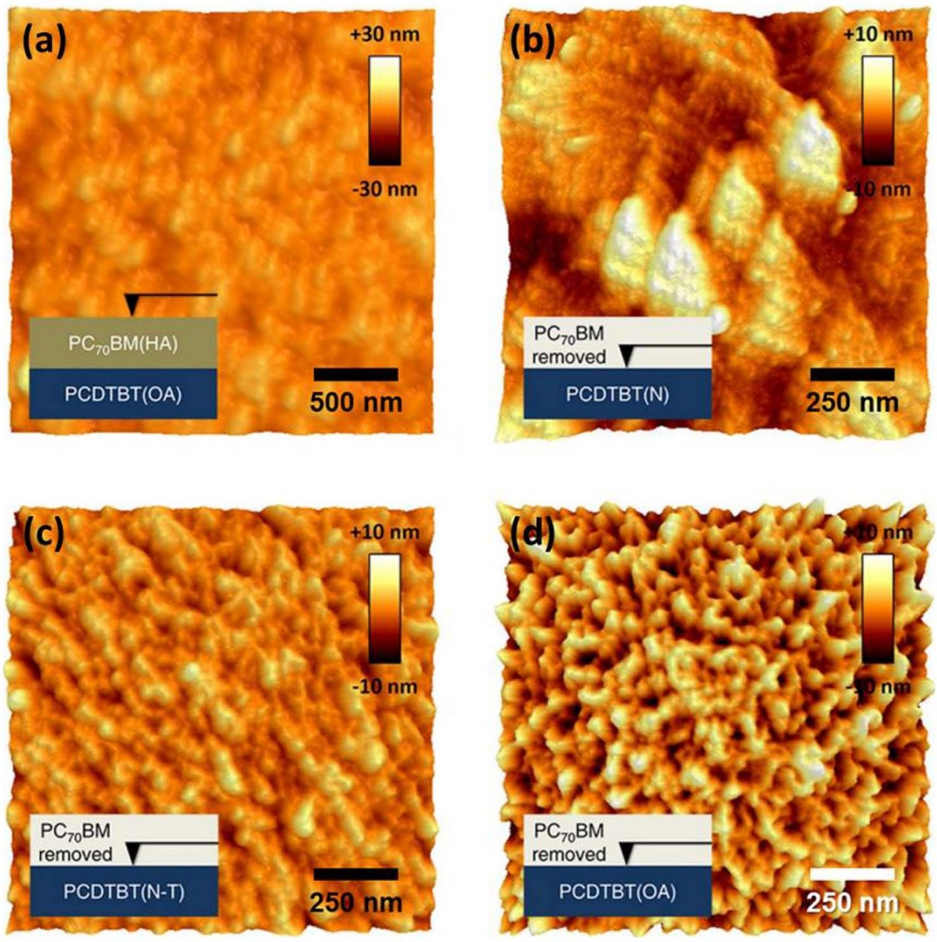

Figure 4 | Surface morphologies of the SD-bilayer of PCDTBT(OA)/PC_{70}BM(HA) and PCDTBT bottom-layers. (a) PCDTBT(OA)/PC_{70}BM(HA) SD-bilayer film, (b) PCDTBT(N) bottom-layer after removal of the PC_{70}BM(HA) top-layer from the PCDTBT(N)/PC_{70}BM(HA) film, (c) PCDTBT(N–T) bottom-layer after removal of the PC_{70}BM(HA) top-layer from the PCDTBT(N–T)/PC_{70}BM(HA) and (d) PCDTBT(OA) bottom-layer after removal of the PC_{70}BM(HA) top-layer from the PCDTBT(OA)/PC_{70}BM(HA). All the images were obtained by AFM in tapping mode ((a): 2.5 μm × 2.5 μm, (b–d): 1 μm × 1 μm).

In order to address these shortcomings, conformal formation of the PC_{70}BM top-layer on the PCDTBT bottom-layer without significant destruction of the PCDTBT bottom-layer is critical. To satisfy this requirement, we introduced a **HA** that helps conformal formation of the PC_{70}BM top-layer without destroying the PCDTBT bottom-layer. The following properties are desirable when considering a suitable **HA**: good solubility for PC_{70}BM with low vapor pressure and little solubility for PCDTBT. In this context, we identified several **HA**s for the PC_{70}BM top-layer. Among the **HA**s, **DIM** was found to be appropriate. PC_{70}BM is highly soluble in **DIM** whereas PCDTBT is not soluble. Additionally, the vapor pressure of **DIM** is low enough for the conformal formation of the PC_{70}BM top-layer on the PCDTBT bottom-layer. According to J. S. Moon *et al.*[23], **DIO** and **DIM** are known to inhibit excessive crystallization of the fullerene, which will reduce the roughness of the PC_{70}BM film. The solubility of PC_{70}BM was greatly improved to above 15 mg/mL by adding 5 vol% of **DIM** to the PC_{70}BM DCM solution. The **DIM** containing solutions exhibited good film forming properties compared to DCM only solutions. The surface roughness of the PCDTBT/PC_{70}BM SD-bilayer film was remarkably reduced by adding **DIM** to the PC_{70}BM solution. Hereafter, the PC_{70}BM top-layer prepared from the DCM solvent with 5 vol% of **DIM** will be denoted as **PC_{70}BM(HA)**. The root mean square roughness (R_q) of the **PCDTBT(OA)/PC_{70}BM(HA)** SD-bilayer film was found to be 2.77 nm (Figure 4a) – about 10 times lower than the R_q of **PCDTBT(OA)/PC_{70}BM(N)** (27.5 nm) in Figure 3a. This clearly shows the effect of **HA** on SD-bilayer film roughness.

In addition to reducing the surface roughness of the PCDTBT/PC_{70}BM SD-bilayer film, maximizing the interfacial area of the PCDTBT/PC_{70}BM heterojunction is desirable when constructing an efficient SD-bilayer OPV. To investigate the heterojunction morphologies of PCDTBT/PC_{70}BM SD-bilayers, cross-section transmission electron microscopy (TEM) was conducted on the **PCDTBT(N–T)/PC_{70}BM(HA)** and **PCDTBT(OA)/PC_{70}BM(HA)** films. Clear interface formation between PCDTBT and PC_{70}BM was not observed in the TEM image of both SD-bilayers when the image was taken at focusing conditions (Figure 5a and 5e). The PCDTBT/PC_{70}BM interfaces became distinguishable after underfocusing the SD-bilayer samples to −15 μm. The prepared **PCDTBT(N–T)/PC_{70}BM(HA)** SD-bilayer showed a clear polymer/PC_{70}BM interface suggesting the formation of a planar heterojunction (Figure 5b). However, a polymer/PC_{70}BM interface was not clearly observed for the **PCDTBT(OA)/PC_{70}BM(HA)** SD-bilayer (Figure 5f). The cross-section TEM sample was mapped for sulfur and carbon by energy dispersive X-ray spectroscopy (EDS) (Figure 5c, 5d, 5g and 5f). Since only PCDTBT contains sulfur, the PCDTBT polymer is expected to lie where sulfur is observed. Sulfur was found only in the PCDTBT layer in **PCDTBT(N–T)/PC_{70}BM(HA)**, which is coincident with the cross-section TEM result. In the **PCDTBT(OA)/PC_{70}BM(HA)** SD-bilayer film, how-

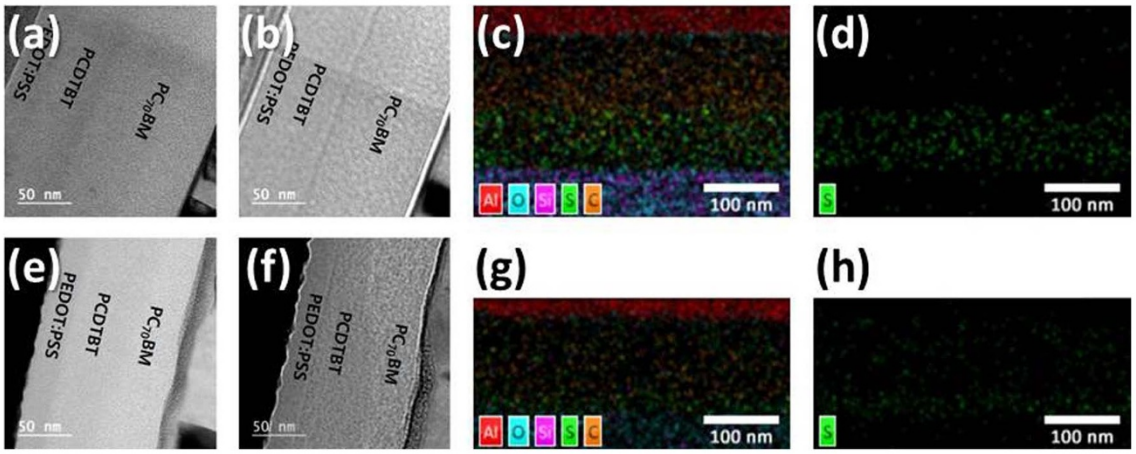

Figure 5 | Cross-section TEM images of the PCDTBT(N–T)/$PC_{70}BM$(HA) SD-bilayer (a, b) and the PCDTBT(OA)/$PC_{70}BM$(HA) SD-bilayer (e, f), and elemental mapping of the corresponding SD-bilayers by EDS (c, d, g and f). (a) Focused cross-section TEM image (b) 15 μm underfocused cross-section TEM image, (c) Al, O, Si, S and C mapping image and (d) S mapping image of the PCDTBT(N–T)/$PC_{70}BM$(HA) SD-bilayer. (e) Focused cross-section TEM image (f) 15 μm underfocused cross-section TEM image, (g) Al, O, Si, S and C mapping image and (h) S mapping image of the PCDTBT(OA)/$PC_{70}BM$(HA) SD-bilayer.

ever, sulfur was found everywhere, and there was a distinct sulfur distribution gradient. The sulfur intensity was most intensive in the PCDTBT bottom-layer, and the intensity decreased in the $PC_{70}BM$ upper-layer. Considering that the spatial resolution of the EDS is larger than the polymer domain size and the AFM image taken of the $PC_{70}BM$ removed **PCDTBT(OA)** layer, it is thought that the PCDTBT and $PC_{70}BM$ domains are interdigitated to form a non-planar heterojunction with a large surface area.

For further investigation into the heterojunction morphology of the PCDTBT/$PC_{70}BM$ SD-bilayers, the $PC_{70}BM$ top-layer was selectively removed from the SD-bilayer films using **DIM** (refer the Film 3 of Figure 1a). And the surface morphology of the $PC_{70}BM$-removed PCDTBT bottom-layer were scanned using AFM and shown in b–d of Figure 4.

Considering both the morphology of the **$PC_{70}BM$(N)** top-layer deposited on the **PCDTBT(OA)** bottom-layer (Figure 3a) and the surface morphology of the **PCDTBT(OA)** bottom-layer after removal of the **$PC_{70}BM$(N)** top-layer (Figure 3d), it was expected that the selective removal of $PC_{70}BM$ by **DIM** would not significantly alter the morphology of the PCDTBT bottom-layer because **DIM** does not dissolve PCDTBT but only selectively dissolves $PC_{70}BM$. We have investigated the effect of the $PC_{70}BM$ removal process on the morphology of the PCDTBT bottom-layer in detail. UV-visible absorption measurement of the DIM solution revealed no absorption from PCDTBT but only absorption due to $PC_{70}BM$ (Figure S1 of Supplementary Information). However, it is difficult to completely remove the $PC_{70}BM$ from the SD-bilayer because the $PC_{70}BM$ is supposed to be inter-diffused into the PCDTBT bottom-layer during the $PC_{70}BM$ top-layer deposition process. To investigate the amount of residual $PC_{70}BM$ left on the PCDTBT bottom-layer, photoluminescence (PL) measurement of the $PC_{70}BM$ removed PCDTBT films were performed. As shown in Figure S2a and b of the Supplementary Information, PL quenching of ~24% was observed for both the **PCDTBT(N–T)** and **PCDTBT(OA)** films after $PC_{70}BM$ removal. Based on the PL quenching experiment for the PCDTBT : $PC_{70}BM$ films with various blending ratios (Figure S2c and d of Supplementary Information), the 24% PL quenching indicates only 0.1 wt% of $PC_{70}BM$ (PCDTBT : $PC_{70}BM$ = 999 : 1) remained in the **PCDTBT(N–T)** and **PCDTBT(OA)** bottom-layers after $PC_{70}BM$ removal with **DIM**. However, the amount of residual $PC_{70}BM$ is thought to be negligible compared to the amount of PCDTBT. Therefore, it is expected that the obtained surface morphology of Figure 4b–d represents the surface morphology of the PCDTBT bottom-layer without any residual $PC_{70}BM$.

However, there is another factor that can influence PCDTBT film morphology. It is possible that **DIM** can cause the PCDTBT to swell changing its morphology. To investigate this, we have examined the surface of the PCDTBT film after several **DIM** treatments. The PCDTBT film was immersed in the **DIM** solution for 10 seconds, and the surface morphology of the PCDTBT film was examined by AFM. As expected, no noticeable change in the film morphology was observed even after repeated DIM treatments (Figure S3 of Supplementary Information).

Based on the above experiments, it was concluded that there is no significant change in the morphology of the PCDTBT bottom-layer during the selective $PC_{70}BM$ removal process, and that the surface morphology of Figure 4b–d represents the morphology of the heterojunction formed at the PCDTBT/$PC_{70}BM$ interface.

There was no significant difference in the surface roughness for the **$PC_{70}BM$(HA)** top-layer removed **PCDTBT(N)**, **PCDTBT(T)** and **PCDTBT(OA)** bottom-layers (3.21 nm, 1.74 nm and 3.37 nm, respectively). However, a significant difference in the surface area was found among the PCDTBT bottom-layers. The surface areas of the films were calculated from the AFM images after excluding the geometric area (1 μm^2) from the total surface area. The surface areas of the **PCDTBT(N)**, **PCDTBT(N–T)** and **PCDTBT(OA)** bottom-layers after removal of the **$PC_{70}BM$(HA)** top-layer were found to be 1.14×10^4 nm^2, 1.34×10^4 nm^2 and 6.60×10^4 nm^2, respectively. The surface areas of **PCDTBT(N)** and **PCDTBT(N–T)** are similar, whereas the surface area of **PCDTBT(OA)** is 6 times larger than the **PCDTBT(N)** bottom-layer and 5 times larger than the **PCDTBT(N)** bottom-layer. This represents a 5–6 fold increase in the heterojunction area of the **PCDTBT(OA)/$PC_{70}BM$(HA)** SD-bilayer compared to the **PCDTBT(N)/$PC_{70}BM$(HA)** and **PCDTBT(N–T)/$PC_{70}BM$(HA)** SD-bilayers. In addition, the surface of the **PCDTBT(OA)** bottom-layer showed a well developed nanoscale morphology compared to the **PCDTBT(N)** and **PCDTBT(N–T)** bottom-layers. The width and height of the **PCDTBT(OA)** domains are around 50 nm and 15 nm, respectively. Considering the outcome of our morphological investigation and surface area calculations at the **PCDTBT(OA)/$PC_{70}BM$(HA)** interface, the **PCDTBT(OA)/$PC_{70}BM$(HA)** is expected to form the most effective non-planar heterojunction for exciton dissociation among the SD-bilayer films.

Cross-section TEM was performed on the $PC_{70}BM$ removed PCDTBT bottom-layers (Figure 6). Aluminum of 10 nm thickness

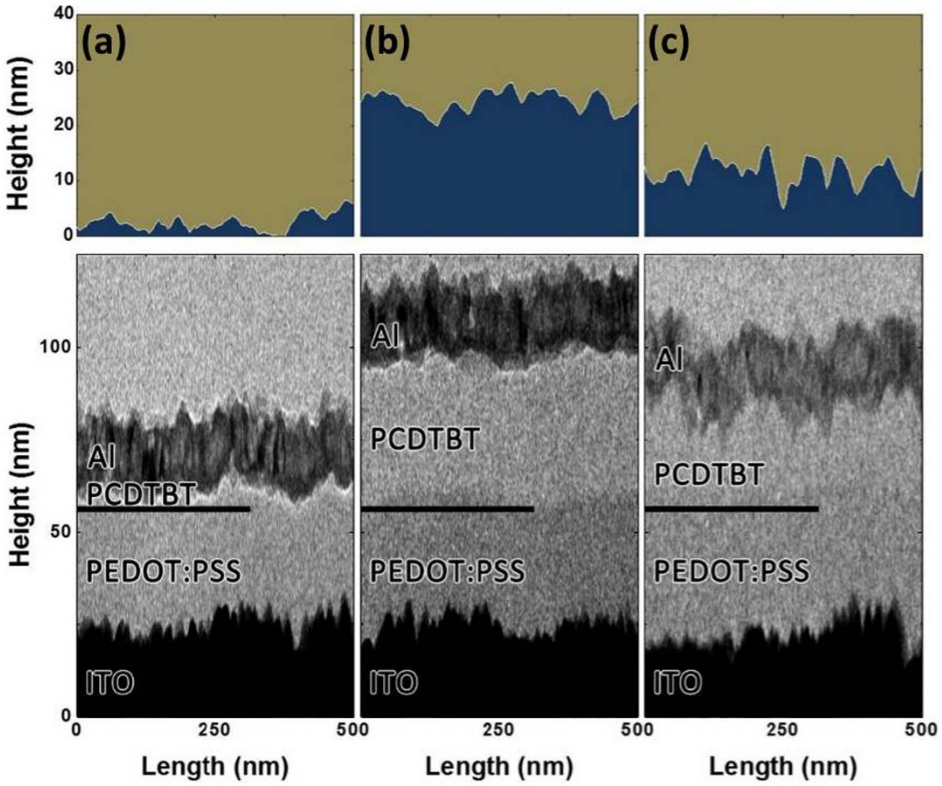

Figure 6 | AFM height profiles and cross-section TEM images of the PCDTBT bottom-layers. (a) PCDTBT(N) bottom-layer, (b) PCDTBT(N–T) bottom-layer and (c) PCDTBT(OA) bottom-layer after removal of the $PC_{70}BM$(HA) top-layer from the corresponding SD-bilayer films. The black horizontal line in the TEM images was inserted for the purpose of indicating the boundary between the PEDOT : PSS and PCDTBT layers.

was thermally evaporated onto the **$PC_{70}BM$(HA)** top-layer removed **PCDTBT(N)**, **PCDTBT(N–T)** and **PCDTBT(OA)** bottom-layers to discern PCDTBT from the background. The TEM images were contracted to the scale of the AFM images (The original TEM images of the films can be found in Figure S4 of Supporting Information), and the TEM results corresponded perfectly with the AFM results. TEM images of the **$PC_{70}BM$(HA)** top-layer removed PCDTBT bottom-layers showed relatively flat profiles for the **PCDTBT(N)** and **PCDTBT(T)** bottom-layers, whereas a rough profile was observed for the **PCDTBT(OA)** bottom-layer. Thus, TEM results support the formation of a non-planar heterojunction with nanoscale morphology in the **PCDTBT(OA)/$PC_{70}BM$(HA)** SD-bilayer film, which is in agreement with the AFM height profile analysis.

Based on the TEM analysis of the SD-bilayers, **PCDTBT(N–T)/$PC_{70}BM$(HA)** forms a SD-bilayer with little inter-diffusion, whereas the $PC_{70}BM$ in the **PCDTBT(OA)/$PC_{70}BM$(HA)** SD-bilayer can penetrate into the amorphous PCDTBT domain and form an inter-diffused bilayer. Consequently, the **PCDTBT(N–T)/$PC_{70}BM$(HA)** SD-bilayer forms a planar heterojunction, and the **PCDTBT(OA)/$PC_{70}BM$(HA)** SD-bilayer forms a non-planar heterojunction with a large surface area.

Figure 7 compares the performance of solar cells having a PCDTBT/$PC_{70}BM$ SD-bilayer processed with an **OA** and **HA**. Their photovoltaic parameters are listed in Table 2. The solar cell performance was significantly enhanced by the incorporation of the **HA** to the $PC_{70}BM$ solution. As expected from the AFM and TEM results, the OPV having a **PCDTBT(OA)/$PC_{70}BM$(HA)** SD-bilayer showed the highest PCE of 7.12% with J_{SC} of 12.02 mA/cm^2, V_{OC} of 0.90 V, and FF of 0.66. The average efficiency of 6.73 $\pm$ 0.14% was obtained from 30 devices. This clearly shows the effect of the **HA** as the OPV fabricated without any **HA**, **PCDTBT(OA)/$PC_{70}BM$(N)**, only exhibited an efficiency of 1.82%. The difference in PCEs of the SD-bilayer OPVs was mainly attributed to the difference in J_{SC}. Among the SD-bilayer OPVs having a **HA** processed top-layer, the **PCDTBT(N)/$PC_{70}BM$(HA)** SD-bilayer showed the lowest J_{SC} and the **PCDTBT(OA)/$PC_{70}BM$(HA)** SD-bilayer OPV showed the highest J_{SC}.

The J_{SC} of a solar cell is affected by the overall carrier dynamics, such as the light absorption efficiency (η_A), the exciton dissociation efficiency (η_{ED}), and the charge collection efficiency (η_{CC})[24]. Comparing η_A of SD-bilayers, the η_A of the **PCDTBT(N)/$PC_{70}BM$(HA)** film will be the lowest among the three different bilayer films. As it was confirmed by the absorption spectra (Figure 1) and TEM (Figure 6a), significant amounts of PCDTBT was removed during the formation of the **$PC_{70}BM$(HA)** top-layer due to a insufficnet ordering of the PCDTBT chains in the **PCDTBT(N)** bottom-layer.

PL measurements on the SD-bilayer films were carried out to investigate the η_{ED} of the SD-bilayer films (Figure S5 of Supplementary Information). The PL of PCDTBT films was quenched to 88.5% and 89.3% after construction of **PCDTBT(N)/$PC_{70}BM$(HA)** and **PCDTBT(OA)/$PC_{70}BM$(HA)** SD-bilayer films, respectively. The PL of **PCDTBT(N–T)/$PC_{70}BM$(HA)** SD-bilayer film, however, shows 81.6% quenching compared to the PL of PCDTBT film. Considering the fact that little amount of $PC_{70}BM$ in PCDTBT film significantly quenches PL intensity of PCDTBT film (Figure S3 of Supplementary Information), the difference in PL intensity between **PCDTBT(OA)/$PC_{70}BM$(HA)** and **PCDTBT(N–T)/$PC_{70}BM$(HA)** is not substantial. Based on the GIXD and TEM results, the thermal annealing enhances the ordering of PCDTBT and results in increased size of ordered PCDTBT domains that prevent penetration of $PC_{70}BM$ into PCDTBT layer. As a result, the **PCDTBT(N–T)/$PC_{70}BM$(HA)** SD-bilayer forms a relatively flat interface compared to the **PCDTBT(OA)/$PC_{70}BM$(HA)** SD-bilayer, which was also confirmed by surface area calculation results in Figure 4c and d. This lowers the η_{ED} of **PCDTBT(N–T)/$PC_{70}BM$(HA)** SD-bilayer films.

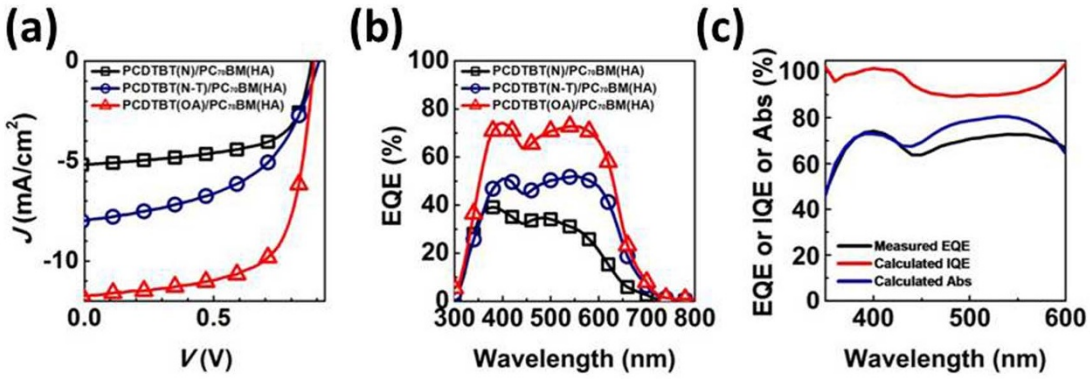

Figure 7 | Performance of SD-bilayer OPVs. (a) current density (J) vs. voltage (V) curves of SD-bilayer OPVs based on the PCDTBT/$PC_{70}BM$ SD-bilayers with different PCDTBT bottom-layers, (b) EQE spectra of the PCDTBT/$PC_{70}BM$ SD-bilayer OPVs and (c) calculated IQE spectrum (red) of the OPV obtained from measured EQE (black) and calculated absorption spectrum (blue) of the PCDTBT(OA)/$PC_{70}BM$(HA) SD-bilayer.

Consequently, the inferior η_A of **PCDTBT(N)/PC_{70}BM(HA)** and the inefficient η_{ED} of **PCDTBT(N–T)/PC_{70}BM(HA)** is considered to be the main reason for the lower J_{SC} of corresponding SD-bilayer OPVs compared to that of **PCDTBT(OA)/PC_{70}BM(HA)** OPV. Although the high efficiency of **PCDTBT(OA)/PC_{70}BM(HA)** is thought to be ascribed to non-planar heterojunction formation with high interfacial area, other factors could also be responsible including changes in the carrier mobility of material on either side of the junction, changes in the interfacial recombination rate due to differences in the orientation of the polymer chains, or changes in the exciton diffusion length.

The maximum external quantum efficiency (EQE) of 72.8% was obtained at 540 nm (Figure 7b). The EQE and PCE values of the SD-bilayer OPV are comparable to the reported EQE and PCE values obtained from the PCDTBT : PC_{70}BM BHJ OPV[11,12]. The IQE of the **PCDTBT(OA)/PC_{70}BM(HA)** OPV device was calculated considering the internal absorption obtained by the reflectance measurement on the device (Figure 7c). The detailed process for the IQE of the SD-bilayer OPV device is described in **Measurements** in the **Methods** section. Briefly, the IQE value of the OPV device was obtained after dividing EQE values of the device by the calculated absorption of the active layer only. The calculated IQE value of the OPV device is in the range of 90% to 100%, which indicates a very efficient charge collection ability for the SD-bilayer OPV device.

Interestingly, the optimized thickness of the PCDTBT bottom-layer of the **PCDTBT(OA)/PC_{70}BM(HA)** SD-bilayer is only around 20 nm (Figure 6c). Considering the optimum thickness of the PCDTBT : PC_{70}BM layer in BHJ OPVs was found to be 80–100 nm, the thickness of the PCDTBT bottom-layer of our SD-bilayer OPV seems relatively thin. However, when considering that the blending ratio of PCDTBT : PC_{70}BM for a BHJ is around 1 : 4, the amount of PCDTBT in our SD-bilayer and the BHJ is similar. The absorption spectrum of the PCDTBT/PC_{70}BM SD-bilayer film almost coincides with that of the BHJ film (PCDTBT : PC_{70}BM = 1 : 4). (Figure S6 of Supporting Information). Furthermore, the absorption intensities of PCDTBT films after removing the PC_{70}BM from the BHJ film and SD-bilayer film are similar. This implies the amount of PCDTBT in the SD-bilayer film is similar with that in the BHJ film. In addition, the reflectance data of the **PCDTBT(OA)/PC_{70}BM(HA)** SD-bilayer device obtained by absorption measurement using a reflective mode clearly shows that light in the range of 350–600 nm is sufficiently absorbed by the **PCDTBT(OA)/PC_{70}BM(HA)** SD-bilayer (Figure S7 in Supporting Information).

Besides **DIO** and **DIM**, we have also tested 1-chloronaphthalene, 3-methylthiophene, 3-hexylthiophene and 1,8-octanedithiol for use as the **OA** or **HA** in the production of the PCDTBT/PC_{70}BM SD-bilayer OPV, and the results are summarized in Figure S8, Figure S9, Table S1 and Table S2 of Supporting Information. Among the PCDTBT/PC_{70}BM SD-bilayer OPVs utilizing **OA** and **HA**, **PCDTBT(DIO)/PC_{70}BM(DIM)** showed the highest PCE.

In conclusion, we have developed a SD-bilayer system of PCDTBT/PC_{70}BM having a non-planar heterojunction with a high interfacial area via solution processes, and we have applied this concept to the construction of highly efficient SD-bilayer OPVs. The construction of the PCDTBT/PC_{70}BM SD-bilayer was achieved by adding the **OA**, for example **DIO**, to the polymer solution. The **OA** improved the ordering of the PCDTBT chains and reduced the solubility of PCDTBT in the top-layer solution. The formation of a nanoscale non-planar heterojunction was achieved by adding the **HA**, for example **DIM**, to the PC_{70}BM solution. The **HA** enabled the conformal deposition of the PC_{70}BM top-layer onto the PCDTBT bottom-layer and enabled the formation of the large area heterojunction. The SD-bilayer OPV utilizing an **OA** and **HA** shows a PCE of 7.12%. We expect that this method can be applied to polymers that are not adequate for use in the BHJ system due to the large surface energy difference between the polymer and fullerene as this difference is not significant in the SD-bilayer system. We believe that our SD-bilayer system establishes an alternative to the BHJ system for the fabrication of efficient OPVs, and also allows for the reassessment of those polymers which have shown insufficient performance in a BHJ system.

Methods

Device fabrications. Pre-patterned ITO-coated glass substrates (20 Ω/□) were cleaned by ultrasonic treatment for 10 min in isopropyl alcohol (IPA), acetone and IPA again then dried at 100°C in a convection oven for 30 min. The cleaned substrates were treated with UV ozone for 20 min. The poly(3,4-ethylenedioxythiophene) : poly(styrenesulfonate) (PEDOT : PSS) (Clevios™ P VP AI 4083, Germany) layer was spin-coated onto the cleaned substrates with a speed of 4000 rpm for 35 s and then dried at 100°C in a vacuum oven for 10 min. A PCDTBT (1-Material, Canada) solution (8 mg/mL) was dissolved in **CB** without **OA** or with 1 vol% of **OA**. For the **OA**, **DIO** (TCI, Japan) was used. The PCDTBT layer was dried at 100°C in a vacuum oven for 15 min after the layer was spin-coated onto the PEDOT : PSS layer with a speed of 2500 rpm for 30 s. A PC_{70}BM (Nano-C, USA) solution (6 mg/mL) was prepared in DCM without **HA** or with 5 vol% of **HA**. **DIM** was used for the **HA**. The PC_{70}BM layer was spin-coated on top of the PCDTBT layer with a speed of 4000 rpm for 30 c and subsequently dried at 100°C in a vacuum oven for 15 min. TiO_2 nanoparticles were dispersed in *n*-butanol with 0.4 wt%. TiO_2 interlayer was deposited onto the PC_{70}BM layer by spin-coating at 1500 rpm for 30 s and dried at 60°C on a hot plate for 30 min. A 100 nm-thick Al metal electrode was thermally evaporated under a pressure of 3.0×10^{-6} Torr.

Measurements. Current density-voltage characteristics were measured by a Keithley 2400 source meter under AM 1.5 G irradiation (100 mW/cm²) from a 150 W Xenon lamp based solar simulator (McScience, Korea). Incident photon-to-current efficiency (IPCE) was measured at different wavelength with a monochromatic light generated from a 300 W Xenon lamp in the range of 300 nm to 800 nm using K3100 EQX (McScience, Korea). UV-visible spectrophotometer UV-2450 (SHIMADZU, Japan) is used to obtain the absorbance spectrum of the films. AFM images were recorded in non-contact mode using XE-70 (Park Systems Corp., Korea) and TEM

images were obtained using Tecnai™ G2 F20 (FEI, USA) with 200 kV accelerating voltage. GIXD measurements were conducted at PLS-II 9A U-SAXS beamline of Pohang Accelerator Laboratory (Korea). The X-rays coming from the in-vacuum undulator (IVU) are monochromated (wavelength $\lambda = 1.114$ Å) using a double crystal monochromator and focused both horizontally and vertically (450 (H) × 60 (V) μm^2 in FWHM @ sample position) using K-B type mirrors. GIXD sample stage is equipped with a 7-axis motorized stage for the accurate alignment and the incidence angle of X-ray beam was set to 0.11° in this study. GIXD patterns were recorded with a 2D CCD detector (Rayonix SX165, USA) and X-ray irradiation time was 5–100 s dependent on the saturation level of detector. Diffraction angles were calibrated by a pre-calibrated sucrose (Monoclinic, P21, $a = 10.8631$ Å, $b = 8.7044$ Å, $c = 7.7624$ Å, $b = 102.938°$) and the sample-to-detector distance was about 243 mm[25]. To estimate the absorption of active layers only and the IQE transfer-matrix formalism (TMF) was used[26,27]. The multilayer structure was assumed to be glass/ITO (120 nm)/PEDOT : PSS (30 nm)/PCDTBT : $PC_{70}BM$ (1 : 4 w/w, 80 nm)/TiO_2 (8 nm)/Al (100 nm). The refractive indices of glass and Al were obtained from Ref. 28 and Ref. 29, respectively, and those of other layers were acquired by ellipsometry.

1. Shaheen, S. E. Radspinner, R. Peyghambarian, N. & Jabbour, G. E. Fabrication of bulk heterojunction plastic solar cells by screen printing. *Appl. Phys. Lett.* **79**, 2996–2998 (2001).
2. Steirer, K. X. *et al.* Ultrasonically sprayed and inkjet printed thin film electrodes for organic solar cells. *Thin Solid Films* **517**, 2781–2786 (2009).
3. Krebs, F. C., Gevorgyan, S. A. & Alstrup, J. A roll-to-roll process to flexible polymer solar cells: model studies, manufacture and operational stability studies. *J. Mater. Chem.* **19**, 5442–5451 (2009).
4. Ayzner, A. L., Tassone, C. J., Tolbert, S. H. & Schwartz, B. J. Reappraising the need for bulk heterojunctions in polymer-fullerene photovoltaics: The role of carrier transport in all-solution-processed P3HT/PCBM bilayer solar cells. *J. Phys. Chem. C* **113**, 20050–20060 (2009).
5. Lee, K. H. *et al.* Morphology of all-solution-processed "bilayer" organic solar cells. *Adv. Mater.* **23**, 766–770 (2011).
6. Moon, J. S., Takacs, C. J., Sun, Y. & Heeger, A. J. Spontaneous formation of bulk heterojunction nanostructures: Multiple routes to equivalent morphologies. *Nano Lett.* **11**, 1036–1039 (2011).
7. Gevaerts, V. S., Koster, L. J. A., Wienk, M. M. & Janssen, R. A. J. Discriminating between bilayer and bulk heterojunction polymer : fullerene solar cells using the external quantum efficiency. *ACS Appl. Mater. Interfaces* **3**, 3252–3255 (2011).
8. Vohra, V. *et al.* Enhanced vertical concentration gradient in rubbed P3HT : PCBM graded bilayer solar cells. *J. Phys. Chem. Lett.* **3**, 1820–1823 (2012).
9. Ayzner, A. L., Doan, S. C., Villers, B. T. & Schwartz, B. J. Ultrafast studies of exciton migration and polaron formation in sequentially solution-processed conjugated polymer/fullerene quasi-bilayer photovoltaics. *J. Phys. Chem. Lett.* **3**, 2281–2287 (2012).
10. Zhao, C. X., Mao, A. L. & Xu, G. Junction capacitance and donor-acceptor interface of organic photovoltaics. *Appl. Phys. Lett.* **105**, 063302 (2014).
11. Park, S. H. *et al.* Bulk heterojunction solar cells with internal quantum efficiency approaching 100%. *Nat. photonics* **3**, 297–303 (2009).
12. Wang, D. H., Kim, J. K., Seo, J. H., Park, O. O. & Park, J. H. Stability comparison: A PCDTBT/$PC_{71}BM$ bulk-heterojunction versus a P3HT/$PC_{71}BM$ bulk-heterojunction. *Sol. Energy Mater. Sol. Cells* **101**, 249–255 (2012).
13. Peters, C. H. *et al.* Highly efficiency polymer solar cells with long operating lifetimes. *Adv. Energy Mater.* **1**, 491–494 (2011).
14. He, Z. *et al.* Enhanced power-conversion efficiency in polymer solar cells using an inverted device structure. *Nat. Photonics* **6**, 591–595 (2012).
15. Bronstein, H. *et al.* Thieno[3,2-*b*]thiophene-diketopyrrolopyrrole containing polymers for inverted solar cells devices with high short circuit currents. *Adv. Funct. Mater.* **23**, 5647–5654 (2014).
16. Osaka, I. *et al.* Synthesis, characterization, and transistor and solar cell applications of a naphthobisthiadiazole-based semiconducting polymer. *J. Am. Chem. Soc.* **134**, 3498–3507 (2012).
17. Sun, B. *et al.* Dramatically enhanced molecular ordering and charge transport of a DPP-based polymer assisted by oligomers through antiplasticization. *J. Mater. Chem. C* **1**, 4423–4426 (2013).
18. Kinder, L., Kanicki, J. & Petroff, P. Structural ordering and enhanced carrier mobility in organic polymer thin film transistors. *Synth. Met.* **146**, 181–185 (2004).
19. Lu, X. *et al.* Bilayer order in a polycarbazole-conjugated polymer. *Nat. Commun.* **3**, 795 (2012).
20. Moon, J. S., Jo, J. & Heeger, A. J. Nanomorphology of PCDTBT : $PC_{70}BM$ bulk heterojunction solar cells. *Adv. Energy Mater.* **2**, 304–308 (2012).
21. Chu, T. Y. *et al.* Morphology control in polycarbazole based bulk heterojunction solar cells and its impact on device performance. *Appl. Phys. Lett.* **98**, 253301 (2011).
22. Baek, S. W. *et al.* Plasmonic forward scattering effect in organic solar cells: A powerful optical engineering method. *Sci. Rep.* **3**, 1726 (2013).
23. Moon, J. S. *et al.* Effect of processing additive on the nanomorphology of a bulk heterojunction material. *Nano Lett.* **10**, 4005–4008 (2010).
24. Forrest, S. R. The limits to organic photovoltaic cell efficiency. *MRS Bulletin* **30**, 28–32 (2005).
25. Hynes, R. C. & Page, Y. L. Sucrose, A convenient test crystal for absolute structures. *J. Appl. Crystallogr.* **24**, 352–354 (1991).
26. Peumans, P., Yakimov, A. & Forrest, S. R. Small molecular weight organic thin-film photodetectors and solar cells. *J. Appl. Phys* **93**, 3693–3723 (2003).
27. Pettersson, L. A. A., Roman, L. S. & Inganas, O. Modeling photocurrent action spectra of photovoltaic devices based on organic thin films. *J. Appl. Phys* **86**, 487–496 (1999).
28. Cho, C. & Lee, J. Y. Multi-scale and angular analysis of ray-optical light trapping schemes in thin-film solar cells: Micro lens array, V-shaped configuration, and double parabolic trapper. *Optics Express* **21**, A276–A284 (2013).
29. Palik, E. D. & Ghosh, G. Handbook of Optical Constants of Solids. (Academic Press, San Diego, 1998).

Acknowledgments

This research was supported by the Global Frontier R&D Program on Center for Multiscale Energy System funded by the National Research Foundation under the Ministry of Science, ICT & Future Planning, Korea. Experiments at PLS-II 9A U-SAXS beamline were supported in part by MIST and POSTECH. This work was supported by the New & Renewable Energy Core Technology Program of the Korea Institute of Energy Technology Evaluation and Planning (KETEP), granted financial resource from the Ministry of Trade, Industry & Energy, Republic of Korea. (No. 20133030011330 and 20133030000210). We thank Prof. Jean Bouffard and Dr. Kris Rathwell for the valuable discussions.

Author contributions

J.S., M.H.K. and K.K. designed the experiments and wrote the manuscript. J.S. carried out the experiments, film and device fabrication and analysis. T.J.S. carried out the 2D-GIXD experiments on the films. C.C. and J.Y.L.carried out the IQE calculation on the OPV device. S.P. and D.Y.R. carried out TEM analysis on the SD-bilayer films. All authors discussed the data and commented on the manuscript.

Additional information

Supplementary information accompanies this paper at http://www.nature.com/scientificreports

Competing financial interests: The authors declare no competing financial interests.

How to cite this article: Seok, J. *et al.* Efficient Organic Photovoltaics Utilizing Nanoscale Heterojunctions in Sequentially Deposited Polymer/fullerene Bilayer. *Sci. Rep.* **5**, 8373; DOI:10.1038/srep08373 (2015).